Letters on Materials 16 (1), 2026 pp. 50-56 www.lettersonmaterials.com

Received 17 October 2025; Accepted 24 November 2025
https://doi.org/10.48612/letters/2026-1-50-56
https://elibrary.ru/yvlarg

Prospects for the application of Ti-Zr-based alloys in a neutron diffraction experiment

P. A. Borisova[1,2], O. V. Strakhov[2], V. A. Sheremetyev[2], A. I. Bazlov[2,3], M. M. Murashev[1], S. S. Agafonov[1], E. R. Khusainova[1,2], I. V. Schetinin[2], S. M. Dubinskiy[†2]

[†]sdubinskiy@gmail.com

[1]National Research Center "Kurchatov Institute", Moscow 123182, Russia
[2]National University of Science and Technology MISIS, Moscow 119049, Russia
[3]St. Petersburg State University, St. Petersburg 199034, Russia

Abstract: Ti-Zr-based alloys have a valuable property: the element ratio can be selected so that the neutron scattering length is reduced to zero, eliminating Bragg reflections. This property makes Ti-Zr-based alloys highly useful in neutron diffraction experiments, where certain devices must be placed directly in the neutron beam. This work studies the potential of as-melted Ti-32.4Zr alloy and thermomechanically treated and laser powder bed fused Ti-18Zr-15Nb shape memory alloy as materials in direct contact with specimens in a neutron beam — for example, in powder containers or pressure gas cells in neutron diffraction experiments. As a result, all tested alloys have no pronounced Bragg reflections of the neutrons. Their linear neutron attenuation coefficient is on similar level and about 1.7 times lower than those of commonly used vanadium. Reference silicon powder can be easily studied by neutron diffraction experiment in a custom-made container of the Ti-32.4Zr alloy with thick (2.5 mm) walls. Functional properties of Ti-32.4Zr and Ti-18Zr-15Nb alloys are on a similar level, while Ti-18Zr-15Nb alloy has a significant advantage due to ease of manufacturing and material availability. Thus, the Ti-18Zr-15Nb shape memory alloy is a promising candidate for devices staying in the direct contact with the specimen and placed in a neutron beam and which should be transparent to neutrons not to affect the results of the experiment, as for example fixtures, the powder container, pressure gas cells, high-pressure cell elements and gaskets in a neutron diffraction experiment.

Keywords: neutron diffraction, X-ray diffraction, neutron attenuation, neutron scattering, high-pressure, Ti-Zr-Nb shape memory alloy, Ti-Zr

Acknowledgments: *Neutron diffraction and radiography studies were performed using the unique scientific facility "Neutron research complex based on the IR-8 reactor" of the National Research Center "Kurchatov Institute". The present work was carried out with the financial support of the Russian Science Foundation, project number 25-19-00871 https://rscf.ru/project/25-19-00871/: thermomechanical treatment, specimen preparation and X-ray diffraction analysis.*

1. Introduction

Ti-Zr-based alloys have a valuable property: the element ratio can be selected so that titanium's negative neutron scattering length is compensated by the positive scattering lengths of alloying elements. This reduces the overall scattering length to zero, eliminating Bragg reflections [1–3]. This property makes Ti-Zr-based alloys highly useful in neutron diffraction experiments, where certain devices must be placed directly in the neutron beam. These devices need to be transparent to neutrons to avoid affecting experimental results — they must have short coherent and incoherent scattering lengths to minimize Bragg diffraction and background signal. Ti-Zr-based alloys are therefore promising materials for fixtures, powder containers, pressure gas cells, high-pressure cell elements, and gaskets [4,5]. Additional requirements are also important for practical applications: high mechanical strength for load-bearing devices (such as high-pressure cell elements and gaskets), as well as ease of manufacturing and material availability [6–13].

The Ti-32.4Zr (at.%) alloy of a conventional binary Ti-Zr system has a zero value of neutron scattering length (b_{coh}) according to its composition [3]. However, this alloy is not used outside neutron diffraction experiments, which limits its availability and raises questions about its manufacturability. In contrast, some Ti-Zr-Nb shape memory alloys (SMAs) can fulfill all these criteria. Ti-18Zr-15Nb (at.%) SMA is widely developed as a promising material for orthopedic applications [14]. The thermomechanical treatment (TMT) of Ti-18Zr-15Nb can effectively control the mechanical properties and increase the strength to the level required for the Ti-Zr alloy [8] designed for the neutron diffraction experiments [3,8,15,16]. Furthermore, Ti-18Zr-15Nb has excellent manufacturability. It is successfully produced in ingots and bar stocks of various cross-sections obtained by TMT [17,18], which can be machined by conventional cutting techniques. Moreover, a three-dimensional product with complex internal channel geometries can be produced by additive manufacturing, since the laser powder bed fusion (LPBF) method was successfully applied to this alloy [19]. This capability is extremely important for manufacturing collimators used at neutron experimental stations. The calculated scattering length (b_{coh}) of Ti-18Zr-15Zr alloy is of 0.043 fm [20], which is nearly zero.

The aim of this work is to study the potential of as-melted Ti-32.4Zr alloy and thermomechanically treated and laser powder bed fused Ti-18Zr-15Nb shape memory alloy as materials in direct contact with specimens in a neutron beam — for example, in powder containers or pressure gas cells in neutron diffraction experiments.

2. Materials and methods

2.1. Materials

As straightly designed for the application in the neutron diffraction filed and the most promising material, binary Ti-32.4Zr (at.%) alloy was obtained, and a powder container was made from it to evaluate the possibility of its practical application. A 250 g ingot of the Ti-32.4Zr alloy was obtained by the vacuum arc melting with a non-consumable tungsten electrode using Arcast arc 200 furnace (Arcast Inc., USA). High-purity titanium and zirconium iodide rods served as initial materials. The ingot was remelted 5 times to achieve a homogeneous chemical composition. The ingot was EDM-cut into blanks, which were then mechanically machined into a custom-made powder container (Fig. 1). The wall thickness of the container is 2.5 mm, the internal space for the powder specimen has a cylindrical shape with a diameter of 3 mm and a height of 10 mm. While such thick walls are not typical for the power containers, this wall thickness is critical for the future transition to pressure gas cells.

The Ti-18Zr-15Nb (at.%) shape memory alloy was obtained in two forms: thermomechanically treated and laser powder bed fused. A 20 kg, 160 mm-diameter ingot was fabricated by vacuum arc melting [18]. The ingot was re-melted at least 4 times to ensure compositional homogeneity. It was subjected to multi-axial hot forging in the 950–1050°C temperature range with a true strain of $e=3.5$ and then machined and ground to a 21.5 mm-diameter bar stock. The bars were rotary forged ($e=2.5$) at 700°C with either air cooling to obtain 6.4 mm-diameter bar specimens. Specimens were hot straightened by tension at 700°C with electrical contact heating and grinded to a 5.4 mm diameter.

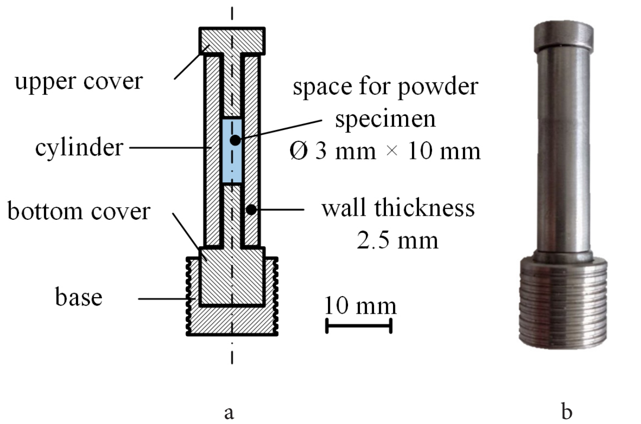

Fig. 1. (Color online) Sectional scheme of the custom-made powder container of Ti-32.4Zr (at.%) alloy (a) and photograph of the assembled container (b).

A Ti-18Zr-15Nb ingot (160 mm diameter, 200 mm long) was produced using vacuum arc melting and subsequently processed by electrode induction gas atomization melting (EIGA) at the NRC "Kurchatov Institute"–VIAM. The resulting powder was sieved to achieve the following particle size distribution: $d_{10}=15.7$ μm, $d_{50}=32.9$ μm, $d_{90}=55.6$ μm [21]. A TruPrint1000 LPBF system equipped with a 200 W ytterbium fiber laser (spot diameter 30 μm) was employed. To print a high-density alloy (≥99.5%), the following parameters were selected: laser power $P=175$ W, scanning speed $v=1420$ mm/s, hatching distance $h=60$ μm, and layer thickness $t=30$ μm [19]. After printing, the cylindrical specimen with 6.0 mm-diameter and 70 mm length was annealed at 800°C for 1 h in vacuum, followed by furnace cooling.

The composition of the main elements was evaluated in initial as melted condition and after SLM (only for Ti-18Zr-15Nb alloy) by EDS analysis via Tescan Vega3 microscope (TESCAN, Czech Republic) and the impurities content was measured using TC-600 analyzer (Leco, Geleen, The Netherlands). The alloys' compositions and the impurities content is presented in Table 1.

As a reference material in the radiography experiment, a commercially evaluable vanadium rode 99.38% purity with width of 5 mm was used as a material commonly used in a neutron diffraction experiment with low neutron scattering length. For the direct evaluation of custom-made powder container of Ti-32.4Zr alloy, silicon powered with 1–10 μm particles size and of 99.999% purity was used in neutron diffraction experiment.

Table 1. Chemical compositions and impurities content in analyzed materials.

Alloys and conditions	Main elements (at.%)			Impurities (wt.%)			
	Ti	Zr	Nb	O	C	H	N
Ti-32.4Zr as melted	main	32.2 ± 0.5	-	0.04	0.03	0.005	0.001
Ti-18Zr-15Nb TMT [18]	main	17.8 ± 0.5	15.1 ± 0.5	0.06	0.03	0.003	0.001
Ti-18Zr-15Nb LPBF [21]	main	18.2 ± 0.5	14.8 ± 0.5	0.17	0.02	0.014	0.001

2.2. Methods

2.2.1. X-Ray diffraction analysis

Since the selected alloys are tend to have a zero scattering length and no Bragg reflections in neutron diffraction experiment, a classical X-Ray diffraction analysis (XRD) was performed for the phase structure evaluation. It was carried out at room temperature by a DRON-4 diffractometer (Russia) with CuK_α radiation ($\lambda_{CuK\alpha}$=1.54178 Å) in the 30 – 90 2θ° range. Plate specimens were cut by diamond saw to a thickness of 1 mm and dimensions of 10×10 mm for the Ti-32.4Zr alloy, and to a diameter of 5.4 mm for the Ti-18Zr-15Nb after TMT and 6 mm for the LPBF. Then they were etched in a $HF:3HNO_3:6H_2O$ solution to remove the mechanically damaged layer. For the direct comparison of XRD results with results of neutron diffraction experiment, the XRD results were plotted in the scattering vector magnitude *Q* calculated using Eq. (1):

$$Q = \frac{4\pi}{\lambda} \cdot \sin\theta, \quad (1)$$

where θ is the scattering angle, °; λ is the wave length, Å.

2.2.2. Neutron diffraction experiment

For the evaluation of possible Bragg reflections of neutrons, the neutron diffraction experiment was conducted at the DISC [22] neutron diffraction station of IR-8 reactor at the NRC "Kurchatov Institute" (Russia). The wave length of monochromatic neutrons was 1.43 Å. The detector system of the ring diffractometer consists of 224 scintillators, the size of the beam collimator (limiter) window is of 5×10 mm. The beam size was chosen to be large enough, but not to exceed the cross-section of the specimens. The central part of a custom-made powder container with an empty or filled space for powder was therefore used for characterizing the Ti-32.4Zr alloy or silicon powder. The length of the Ti-18Zr-15Nb specimens was 50 mm after TMT and 20 mm after LPBF. The exposure time ranged for 1 to 12 hours. The neutron diffraction graphs were plotted as the dependence of neutron diffraction intensity from the scattering vector magnitude *Q*.

2.2.3. Radiography

To evaluate the neutron scattering length, the neutron transmission studies were conducted at the DRAGON [23] neutron imaging station of IR-8 reactor at the NRC "Kurchatov Institute" (Russia). An indirect registration detector from Neutron Optics with replaceable scintillator plates was used as a detector system at the DRAGON station. During the study, neutron radiation of the thermal spectrum hit the scintillator and converted into visible light and recorded by ATIK-4000 camera (Kodak KAI 04022 CCD sensor + Nikon 50 mm f/1.2 lens) with the resolution 2048×2048 pixels. The dynamic range of the obtained digital images is of 16 bits. The spatial resolution of the detector is ≈200 μm. To compare different specimens inter se, the linear attenuation coefficient (μ) was calculated using Eq. (2) [24]:

$$\mu = -\ln\left(\frac{I_S - I_{BG}}{I_0 - I_{BG}}\right) / x, \quad (2)$$

where *x* is specimen thickness, cm; I_S is the beam intensity passing through the specimen, a.u.; I_0 is the beam intensity without specimen, a.u.; I_{BG} is the detector background intensity (in the absence of a neutron beam), a.u.

3. Results and discussion

3.1. The X-Ray and the neutron diffraction experiments

3.1.1. Ti-32.4Zr alloy

Based on the XRD results, the phase composition of the Ti-32.4Zr alloy is represented only by the hexagonal close-packed (HCP) α-phase at room temperature (see Fig. 2). It should be noted, that 112_α and 201_α lines exhibit significantly higher intensity than 100_α, 101_α, 102_α, 110_α and 103_α lines, which is not typical for non-textured HCP lattices. Such crystallographic texture can be a result of oriented crystallization process after smelting.

According to the neutron diffraction data, the Ti-32.4Zr alloy has two atypical behavior features. First feature is pronounced oscillations visible in the range *Q* from 1 to 4 $Å^{-1}$.

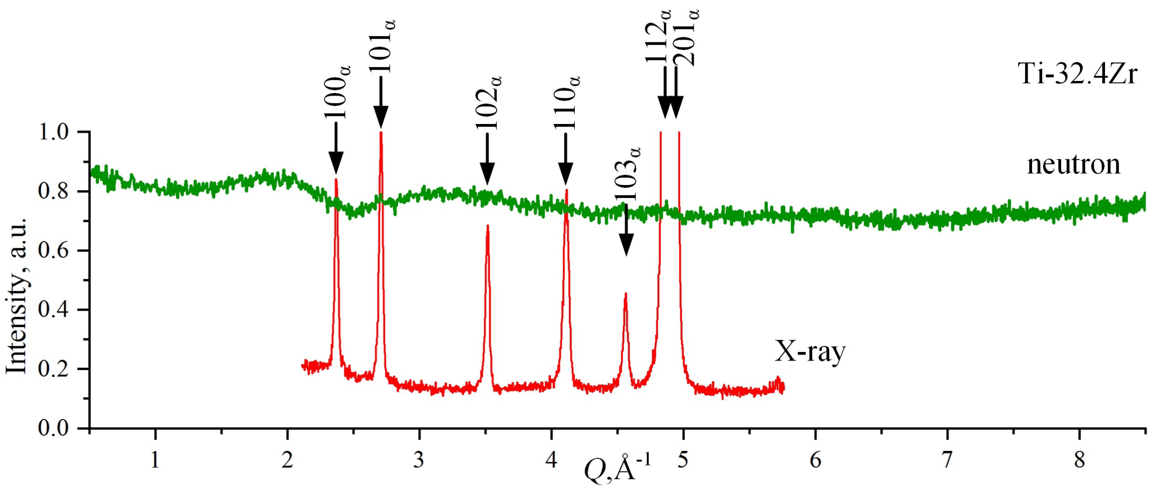

Fig. 2. (Color online) Results of X-Ray and the neutron diffraction experiments of Ti-32.4Zr alloy.

The second feature is the lack of pronounced Bragg reflections, which is due to a zero value of neutron scattering length (b_{coh}). The oscillations may be related to the short range species-species order i.e. preferential surrounding of Ti atoms by Zr atoms of or vice versa [3]. Furthermore, non-ideal stoichiometry on a very local scale could create the volumes with neutron scattering length differ from zero and affect the background profile and even gives very weak and wide Bragg reflections [3]. Such local alloy inhomogeneity is related to the as melted condition of the Ti-Zr alloy.

3.1.2. Ti-18Zr-15Nb shape memory alloy

Main phase in Ti-18Zr-15Nb shape memory alloy is a body-centered cubic(BCC) β-phase at room temperature in accordance with XRD results (Fig. 3). Some weak peaks of HCP orthorhombic α′′- and HCP α-phases can be also observed: $020_{\alpha''}$, $111_{\alpha''}$ and $021_{\alpha''}$ lines of α′′-phase after TMT (see Fig. 3a) and $111_{\alpha''}$, $130_{\alpha''}$, $132_{\alpha''}$ lines of α′′-phase and 100_{α}, 101_{α}, 102_{α}, 110_{α}, 112_{α} lines of α-phase after LPBF (see Fig. 3b). The presence of α′′- and α-phases could be a feature of the alloy as a result of selected thermomechanical or thermal treatment routes [17].

The neutron diffraction profile of the Ti-18Zr-15Nb shape memory alloy (Fig. 3) shows the oscillations in the Q range from 1 to 8 Å^{-1} without distinct Bragg reflections close to those for the Ti-32.4Zr alloy. Therefore, it can be concluded that calculated scattering length $b_{coh} = 0.043$ fm is still too small to produce the visible Bragg reflections. However, the neutron diffraction profile of the Ti-18Zr-15Nb alloy obtained by LPBF (Fig. 3b) is different form the TMT one (Fig. 3a). It could be explained by are presence of $TiO_{2(a)}$, $TiO_{2(r)}$, ZrO_2, Nb_2O_5 and NbO_2 oxides [25] in the Ti-18Zr-15Nb alloy obtained by LPBF in the amount not sufficient enough for the XRD detection. However, these oxides still do not produce high-intensity parasitic diffraction peaks (Fig. 3b). All these make Ti-18Zr-15Nb shape memory alloy similar to the Ti-32.4Zr alloy in terms of neutron diffraction experiment. Despite the high oscillation at the lower values of the Q magnitude vector and the unexpressed Bragg reflections, they will not affect the results high neutron scattering by studied powder specimen in the container made of Ti-32.4Zr or Ti-18Zr-15Nb alloys. It is explained by the fact that the neutron reflection intensity of the commonly analyzed powders will be several orders of higher than that of oscillations' amplitude for the alloy. However, the thickness of a container's wall will affect the number of neutrons detected.

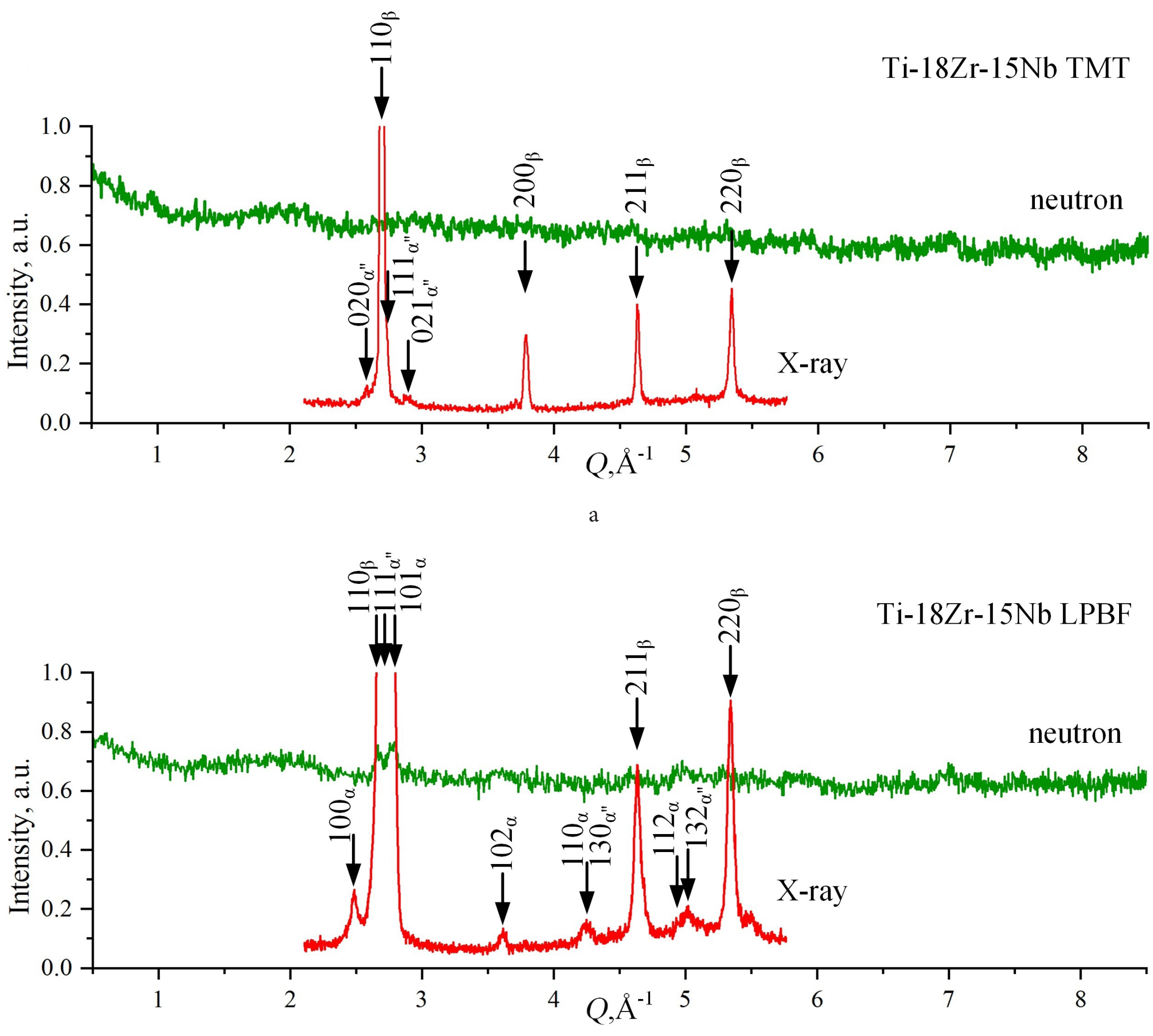

Fig. 3. (Color online) Results of X-Ray and the neutron diffraction experiments of the Ti-18Zr-15Nb shape memory alloy in two forms: after TMT (a) and after LPBF (b).

3.2. The radiography

Since the neutron diffraction profile and absence of pronounced Bragg reflections is not the only important characteristic, but also the neutron attenuation is of high importance, the comparative radiography experiment is performed. The vanadium rode was selected in addition to Ti-32.4Zr and Ti-18Zr-15Nb alloys as a reference specimen due to it has a low coherent and incoherent scattering cross-section and is the most common material for the powder containers [26]. The results of radiography experiment are shown in Fig. 4 which demonstrates the radiographic images of alloys and an example of plotting the neutron transmission graph along a profile section.

All specimens have different cross-sections, therefore the linear neutron attenuation coefficient (cm^{-1}) are calculated based on the neutron transmission graphs in Fig. 4 using Eq. (2) from Section 2.2. The measured neutron transmission values and calculated linear attenuation coefficient are shown in Table 2.

It can be seen from Table 2, that the linear neutron attenuation coefficient (μ) of Ti-32.4Zr and Ti-18Zr-15Nb alloys is very close and differ almost within the error limits. Thus Ti-32.4Zr alloy has linear attenuation coefficient of 0.44 ± 0.01 cm^{-1}, while Ti-18Zr-15Nb alloy has one after LPBF of 0.45 ± 0.01 cm^{-1} and a little bit higher after TMT: $\mu = 0.47 \pm 0.01$ cm^{-1}. However, all these values for Ti-32.4Zr and Ti-18Zr-15Nb alloys are almost 1.7 times lower than that of vanadium, where $\mu = 0.77 \pm 0.01$ cm^{-1}. Therefore, containers made of Ti-32.4Zr and Ti-18Zr-15Nb alloys will attenuate neutrons less than a vanadium alloy container with the same wall thickness, or can be made with 1.7 times thicker walls, which could be important for the high-pressure cells or pressure gas cells [4].

3.3. Custom-made powder container testing

Since the absence of the pronounced Bragg reflections and low linear attenuation coefficient of studied Ti-32.4Zr and Ti-18Zr-15Nb alloys, a direct use of custom-made powder container should be performed in the experimental procedure in order to evaluate the possibility of the real application. With this purpose, a custom-made powder container of Ti-32.4Zr alloy was filled up with silicon powder subjected to the neutron diffraction experiment, and the results of scanning are shown in Fig. 5. It is clearly seen that all characteristic Bragg reflections of silicon are visible and exceed the background level. Indeed the intensity of the characteristic Bragg reflections above the background level is not very high due to uncommonly thick walls (2.5 mm) of the container. However, this wall thickness should be more suitable for the pressure gas cells [4].

Table 2. The neutron transmission values and linear neutron attenuation coefficient for the studied specimens.

Specimen	$I_0 - I_{BG}$, a.u.	$I_S - I_{BG}$, a.u.	Transmission, %	Thickness, mm	μ, cm^{-1}
Ti-32.4Zr	38500 ± 100	27000 ± 100	70.1 ± 0.5	8.00 ± 0.05	0.44 ± 0.01
Ti-18Zr-15Nb (TMT)	38500 ± 100	29900 ± 100	77.7 ± 0.5	5.40 ± 0.05	0.47 ± 0.01
Ti-18Zr-15Nb (LPBF)	38500 ± 100	29400 ± 100	76.4 ± 0.5	6.00 ± 0.05	0.45 ± 0.01
Vanadium	38300 ± 100	26000 ± 100	67.9 ± 0.5	5.00 ± 0.05	0.77 ± 0.01

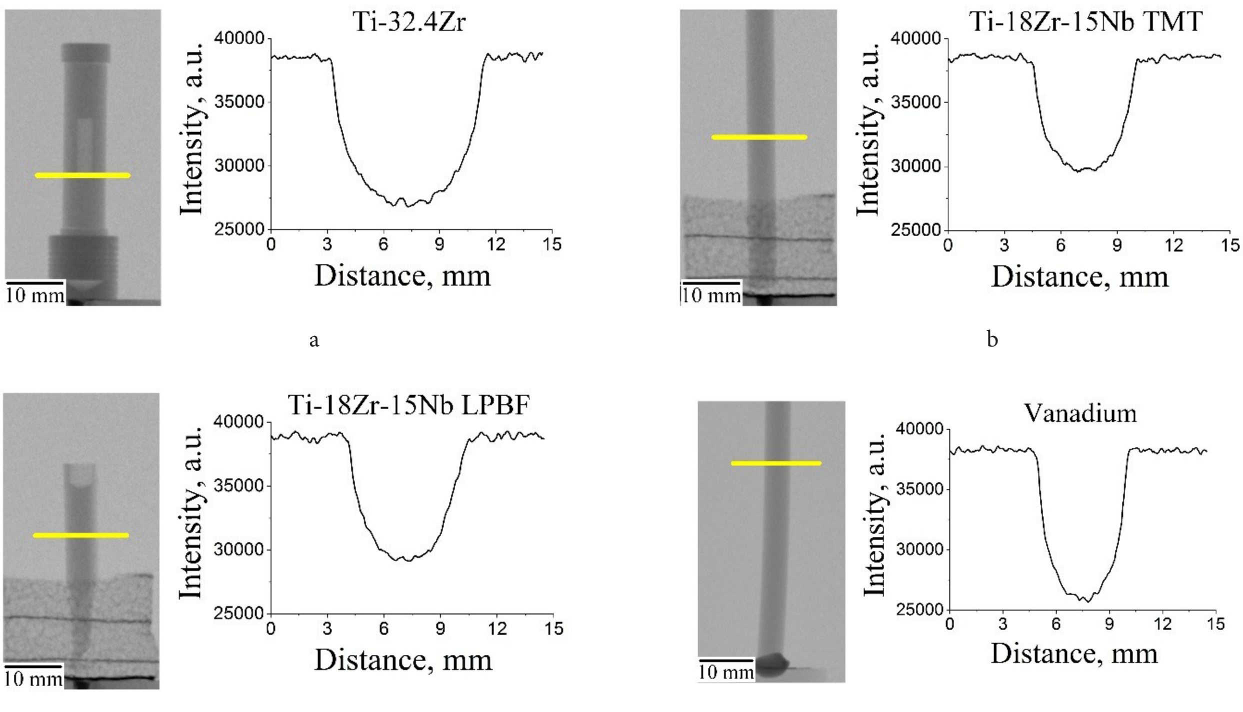

Fig. 4. (Color online) Radiographic images of alloys and an example of plotting the neutron transmission graph along a profile section (yellow line): Ti-32.4Zr alloy (a); Ti-18Zr-15Nb alloy after TMT (b) and after LPBF (c); vanadium (d).

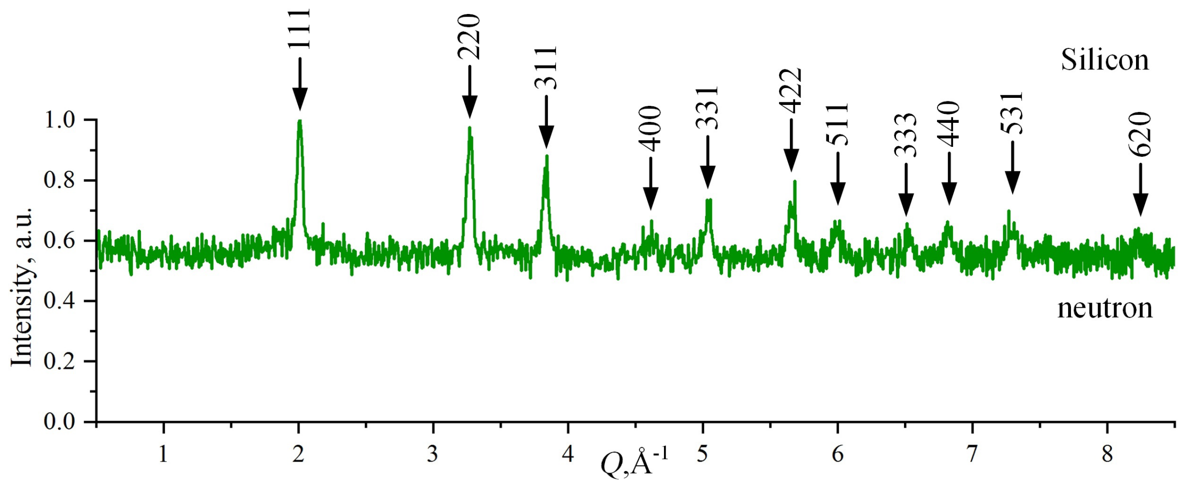

Fig. 5. (Color online) Results of the neutron diffraction experiment of silicon powder in the container made of Ti-32.4Zr alloy.

Furthermore, it is very important that mechanical properties of the Ti-18Zr-15Nb shape memory alloy can be tuned in a wide range, and the high strength can be achieved via TMT or LPBF [21,27], which is close to the strength of Ti-Zr alloys [3], as seen from Table 3. The thermomechanical treatment itself can adjust the mechanical properties of the Ti-18Zr-15Nb alloy over a wide range through the formation of an appropriate structure state. The formation of a recrystallized coarse-grained state corresponds to moderate alloy strength ($\sigma_{0.2}$ = 440 – 470 MPa, UTS = 570 – 640 MPa) but with excellent ductility (δ = 18 – 21%). In contrast, the formation of an age-hardened state increases strength ($\sigma_{0.2}$ = 850 – 1220 MPa, UTS = 870 – 1250 MPa), but decreases ductility to δ = 5 – 12%. These values exceed those of the Ti-32.4Zr alloy: $\sigma_{0.2}$ = 545 – 700 MPa, UTS = 700 – 840 MPa and δ = 8%. The strength of the Ti-18Zr-15Nb alloy produced by LPBF are not exceptionally high: σ_{tr} = 292 MPa, σ_{diss} = 683 MPa, UTS = 725 MPa. This is lower than that of the Ti-32.4Zr alloy. However, its initially high ductility (δ = 16%) creates an opportunity to increase the strength of the LPBF alloy through additional age-hardening. Therefore, both alloys have similar functional properties, while Ti-18Zr-15Nb alloy has a significant advantage due to ease of manufacturing and material availability. This fact along with unique behavior in the neutron beam allow Ti-18Zr-15Nb alloy to be considered as the most promising a material for producing high-pressure cells.

Table 3. Mechanical properties of Ti-18Zr-15Nb and Ti-32.4Zr alloys [3,21,27].

Alloy	$\sigma_{0.2}$, MPa	UTS, MPa	δ, %
Ti-32.4Zr [3]	545 – 700	700 – 840	8
Ti-18Zr-15Nb (age-hardened state) [27]	850 – 1220	870 – 1250	5 – 12
Ti-18Zr-15Nb (recrystallized coarse grained state) [27]	440 – 470	570 – 640	18 – 21
Ti-18Zr-15Nb (LPBF) [21]	292 / 683*	725	16.5

*Transformation/dislocation yield stress

4. Conclusion

The neutron diffraction experiment and neutron radiography of as-melted Ti-32.4Zr alloy and thermomechanically treated and laser powder bed fused Ti-18Zr-15Nb shape memory alloy shown that: (1) all tested alloys have no pronounced Bragg reflections of the neutrons; (2) their linear neutron attenuation coefficient is at similar level and about 1.7 times lower than those of commonly used vanadium; (3) reference silicon powder can be easily studied by neutron diffraction experiment in a custom-made container of Ti-32.4Zr alloy with thick (2.5 mm) walls. All these makes Ti-18Zr-15Nb shape memory alloy a promising candidate for devices staying in the direct contact with the specimen and placed in a neutron beam and which should be transparent to neutrons not to affect the results of experiment, as for example fixtures, the powder container, pressure gas cells, high-pressure cell elements and gaskets in a neutron diffraction experiment.

References

1. S.S. Sidhu, L. Heaton, D.D. Zauberis, F.P. Campos, Neutron Diffraction Study of Titanium-Zirconium System, J. Appl. Phys. 27 (1956) 1040 – 1042.
2. W.G. Marshall, D.J. Francis, Attainment of near-hydrostatic compression conditions using the Paris–Edinburgh cell, Appl. Crystallogr. 35 (2002) 122 – 125.
3. S. Klotz, Techniques in high pressure neutron scattering, CRC press, 2012.
4. I.F. Bailey, A review of sample environments in neutron scattering, Zeitschrift Für Krist. Mater. 218 (2003) 84 – 95.
5. A. Zeidler, M. Guthrie, P.S. Salmon, Pressure-dependent structure of the null-scattering alloy $Ti_{0.676}Zr_{0.324}$, High Press. Res. 35 (2015) 239 – 246.
6. C.J. Ridley, K.V. Kamenev, High pressure neutron and X-ray diffraction at low temperatures, Zeitschrift Für Krist. Mater. 229 (2014) 171 – 199.
7. T. Okuchi, A. Hoshikawa, T. Ishigaki, Forge-hardened TiZr null-matrix alloy for neutron scattering under extreme conditions, Metals (Basel). 5 (2015) 2340 – 2350.
8. A.G. Imgram, D.N. Williams, H.R. Ogden, Tensile

properties of binary titanium-zirconium and titanium-hafnium alloys, J. Less Common Met. 4 (1962) 217–225.
9. Q. Zhao, T. Ueno, N. Wakabayashi, A review in titanium-zirconium binary alloy for use in dental implants: Is there an ideal Ti-Zr composing ratio?, Jpn. Dent. Sci. Rev. 59 (2023) 28–37.
10. J.M. Besson, R.J. Nelmes, G. Hamel, J.S. Loveday, G. Weill, S. Hull, Neutron powder diffraction above 10 GPa, Phys. B Condens. Matter. 180 (1992) 907–910.
11. S. Klotz, J.M. Besson, G. Hamel, R.J. Nelmes, J.S. Loveday, W.G. Marshall, R.M. Wilson, Neutron powder diffraction at pressures beyond 25 GPa, Appl. Phys. Lett. 66 (1995) 1735–1737.
12. J. Xu, Y. Ding, S.D. Jacobsen, H.K. Mao, R.J. Hemley, J. Zhang, J. Qian, C. Pantea, S.C. Vogel, D.J. Williams, Powder neutron diffraction of wüstite ($Fe_{0.93}O$) to 12 GPa using large moissanite anvils, High Press. Res. 24 (2004) 247–253.
13. D.N. Williams, R.A. Wood, R.I. Jaffee, H.R. Ogden, The effects of zirconium in titanium-base alloys, J. Less-Common Met. 6 (1964) 219–225.
14. H.Y. Kim, J. Fu, H. Tobe, J.I. Kim, S. Miyazaki, Crystal structure, transformation strain, and superelastic property of Ti-Nb-Zr and Ti-Nb-Ta alloys, Shape Mem. Superelasticity. 1, 2 (2015) 107–116.
15. S. Li, M. Choi, T. Nam, Effect of thermo-mechanical treatment on microstructural evolution and mechanical properties of a superelastic Ti-Zr-based shape memory alloy, Mater. Sci. Eng. A. 789 (2020) 139664.
16. M. Isaenkova, Y. Perlovich, E. Efimova, D. Zhuk, O. Krymskaya, Superelasticity of Ti-Nb-Zr alloys and their medical application, Mater. Sci. Forum, Trans. Tech. Publ. 879 (2017) 2561–2566.
17. V. Sheremetyev, K. Lukashevich, A. Kreitcberg, A. Kudryashova, M. Tsaturyants, S. Galkin, V. Andreev, S. Prokoshkin, V. Brailovski, Optimization of a thermomechanical treatment of superelastic Ti-Zr-Nb alloys for the production of bar stock for orthopedic implants, J. Alloys Compd. 928 (2022) 167143.
18. K. Lukashevich, V. Sheremetyev, A. Komissarov, V. Cheverikin, V. Andreev, S. Prokoshkin, V. Brailovski, Effect of cooling and annealing conditions on the microstructure, mechanical and superelastic behavior of a rotary forged Ti-18Zr-15Nb (at.%) bar stock for spinal implants, J. Funct. Biomater. 13 (2022) 259.
19. V. Brailovski, V. Kalinicheva, M. Letenneur, K. Lukashevich, V. Sheremetyev, S. Prokoshkin, Control of density and grain structure of a laser powder bed-fused superelastic Ti-18Zr-14Nb alloy: simulation-driven process mapping, Metals (Basel). 10 (2020) 1697.
20. NIST Center for Neutron Research, (2021). Available online
21. V. Sheremetyev, V. Lezin, K. Lukashevich, S. Prokoshkin, V. Brailovski, Improving superelasticity of a laser powder bed-fused Ti-Zr-Nb alloy via the ingot composition adjustments, Mater. Lett. (2025) 138872.
22. V.P. Glazkov, I.V Naumov, V.A. Somenkov, S.S. Shilshtein, Superpositional many-detector systems and neutron diffraction of microsamples, Nucl. Instruments Methods Phys. Res. Sect. A Accel. Spectrometers, Detect. Assoc. Equip. 264 (1988) 367–374.
23. V.A. Somenkov, V.P. Glazkov, V.T. Em, A.I. Gureev, M.M. Murashev, R.A. Sadykov, S.N. Aksenov, D.N. Trunov, A.A. Stolyarov, A.A. Alekseev, Installation for complex radiation diagnostics "DRAGON", Surface. X-Ray, Synchrotron Neutron Res. (2019) 93–99.
24. H.D. Tyufyakov, A.S. Shtan', Fundamentals of Neutron Radiography, Atomizdat, Moscow, 1975.
25. R. Farrakhov, O. Melnichuk, E. Parfenov, V. Mukaeva, A. Raab, V. Sheremetyev, Y. Zhukova, S. Prokoshkin, Comparison of biocompatible coatings produced by plasma electrolytic oxidation on cp-Ti and Ti-Zr-Nb superelastic alloy, Coatings. 11 (2021) 401.
26. M. Potter, H. Fritzsche, D.H. Ryan, L.M. D. Cranswick, Low-background single-crystal silicon sample holders for neutron powder diffraction, Appl. Crystallogr. 40 (2007) 489–495.
27. K. Lukashevich, A. Komissarov, V. Andreev, S. Prokoshkin, V. Sheremetyev, Comparative Study of Mechanical and Functional Properties of Age-Hardened Superelastic Ti-Zr-Nb Alloy with Different Initial Microstructures, Shape Mem. Superelasticity 10 (2024) 392–406.